Available online at www.sciencedirect.com
ScienceDirect
Deep-Sea Research II 54 (2007) 961–980
DEEP-SEA RESEARCH PART II
www.elsevier.com/locate/dsr2

Characteristics of two counter-rotating eddies in the Leeuwin Current system off the Western Australian coast

Ming Feng[a,*], Leon J. Majewski[b], C.B. Fandry[a], Anya M. Waite[c]

[a]CSIRO Marine and Atmospheric Research, Underwood Avenue, Floreat, WA 6014, Australia
[b]Department of Imaging and Applied Physics, Curtin University of Technology, Bentley, WA 6102, Australia
[c]Centre for Water Research, University of Western Australia, Nedlands, WA 6907, Australia

Received 1 September 2005; received in revised form 1 July 2006; accepted 4 November 2006
Available online 18 June 2007

Abstract

A multi-disciplinary R.V. *Southern Surveyor* cruise was conducted in October 2003 to quantify upper ocean productivity within two adjacent, counter-rotating mesoscale eddies (an eddy pair off the coast of Western Australia (WA)) in the southeast Indian Ocean. In this study, a combination of satellite data (altimeter, sea surface temperature, and chlorophyll *a*) and shipboard measurements (acoustic Doppler current profiler (ADCP) and conductivity-temperature-depth (CTD)) were used to characterize the temporal evolution and spatial structures of the eddy pair. Satellite data show that the eddy pair evolved from meander structures of the poleward-flowing Leeuwin Current (LC) in May 2003 and fully detached from the current in late August–early September. Gaussian fits to the ADCP velocities show that the anticyclonic eddy had a maximum azimuthal velocity of 65 cm s^{-1} at 63 km from the eddy centre (the apparent radius), and the cyclonic eddy had a maximum azimuthal velocity of 60 cm s^{-1} at the apparent radius of 49 km. The mixed-layer temperature and salinity properties in the cores of the eddy pair were quite stable over the period of the cruise. Temperature–salinity diagrams indicate that the mixed-layer water in the core of the anticyclonic eddy was composed mainly of LC water, while in the core of the cyclonic eddy the mixed layer water was similar to surrounding open-ocean water. The total volume of the LC water retained in the anticyclonic eddy was 5.6×10^{12} m^3, equivalent to 19 days' annual mean transport of the LC. The chlorophyll *a* concentration in the surface layer of the anticyclonic eddy (LC water) was higher than in the cyclonic eddy (open-ocean water), which was likely a result of the entrainment of the productive water from the continental shelf during the eddy formation stage. The offshore transport of the chlorophyll *a* biomass may be important for the pelagic ecosystem off the coast of WA.

Keywords: Leeuwin Current; Mesoscale eddies; Cross-shelf transport

1. Introduction

The oceanography off the west coast of Western Australia (WA) in the southeast Indian Ocean is unique among the eastern boundary current systems due to the existence of an anomalously large meridional pressure gradient that drives the poleward-flowing Leeuwin Current (LC; Cresswell and Golding, 1980; Godfrey and Ridgway, 1985). The onshore geostrophic flows that supply the LC transport suppress wind-driven upwellings that would otherwise supply nutrients to the surface

*Corresponding author. Tel.: +61 8 9333 6512; fax: +61 8 9333 6555.
E-mail address: Ming.Feng@csiro.au (M. Feng).

0967-0645/$ - see front matter © 2007 Elsevier Ltd. All rights reserved.
doi:10.1016/j.dsr2.2006.11.022

layer in these regions (Thompson, 1987). This renders the oligotrophic marine environment in large parts of the continental shelf region and open-ocean off WA.

The LC increases its current speed and volume transport in austral autumn due to the relaxation of the opposing longshore wind (Feng et al., 2003). The stronger speed leads to intense instability of the current, and large meanders are observed along the path of the current during May–July, as indicated by the seasonal peak of eddy kinetic energy off the southwest WA coast (Fig. 1). Long-lived warm-core eddies tend to form from the meanders of the LC and propagate offshore during austral winter (Fang and Morrow, 2003), consistent with the offshore migration of the high eddy kinetic energy with seasons (Fig. 1). We refer the region of high mean flow and eddy energetics off the coast of WA as the "LC system". The LC system possesses the highest surface eddy kinetic energy among all the mid-latitude eastern boundary current systems (Feng et al., 2005). Seasonal increases of sea surface chlorophyll *a* (SSC) biomass in the LC system are observed in satellite data during late austral autumn to early winter (May–July), which lead the general late winter peak in the open ocean (Fig. 2; see also Moore et al., 2007).

Cyclonic eddies have been suggested to generate large productivity pulses in the open ocean (Falkowski et al., 1991; McGillicuddy et al., 1999; Bidigare et al., 2003), especially in nutrient-poor waters. Anticyclonic eddies can support production at their centres (Crawford et al., 2005) or at their perimeters (Franks et al., 1986; Mizobata et al., 2002) due to advection and mixing processes. Anticyclonic eddies also can entrain high productivity water from coastal regions into their outer rings (Crawford et al., 2005). To assess the roles of mesoscale eddies on nutrient "pumping" off the coast of WA, two counter-rotating eddies are sampled during a multi-disciplinary R.V. *Southern Surveyor* cruise in October 2003 to document in detail the productivity and biophysical coupling in the eddies at their mature stage (Fig. 3). Both satellite and cruise data show that there is less chlorophyll *a* biomass in the cyclonic eddy than the anticyclonic eddy, suggesting different roles of mesoscale eddies in the biological processes in the LC system. The present study describes the temporal evolution of the eddy pair from the LC and characterises the physical structures of the two eddies, in order to help the analyses of biogeochemical data sampled during the cruise (Waite et al., 2007). This study also investigates the water mass properties of the two eddies and discusses possible roles of mesoscale eddies in enhancing chlorophyll *a* biomass in the pelagic ecosystem off the coast of WA.

2. Data

An altimeter sea-level anomaly product based on the combined TOPEX Poseidon (Jason-1) and ERS-1/ERS-2 (Envisat) satellite missions from October 1992 to present was obtained from CLS Space Oceanography Division (Le Traon et al., 1998; Ducet et al., 2000). The product is mapped on a 7-day temporal and a 1/3° Mercator spatial grid, with a temporal correlation scale of 15 days and spatial correlation scale of about 175 km (at 30°S). A real-time version of the product was used to track the evolution of eddies off the coast of WA before and during October 2003 *Southern Surveyor* cruise (D. Griffin, personal communication).

SSC products from the moderate resolution imaging spectroradiometer aboard the Aqua platform (MODIS-Aqua) and the sea-viewing wide field-of-view sensor (SeaWiFS) were acquired from NASA for the period of the research cruise, as well as throughout the lifetime of the eddy pair. These data have a spatial resolution of 1 km and temporal resolution of approximately 1 day. Advanced very high resolution radiometer (AVHRR) and MODIS-Aqua sea-surface temperature (SST) products were obtained for the corresponding dates. The SSC and SST data were used to visually track the eddy movements and estimate the chlorophyll *a* biomass of the two eddies.

The *Southern Surveyor* cruise was carried out in two stages, sampling the anticyclonic eddy during October 1–11 and then sampling the cyclonic eddy during October 12–22 after a short port call (Fig. 3A). A shipboard acoustic Doppler current profiler (ADCP) was operated during the cruise to measure the ocean current from 19 m to about 251 m depth in 8-m bins. The mean positions of the two eddies were 31°8.1′S, 111°46.1′E and 31°0.8′S, 109°55.1′E (Fig. 3B; Table 1), as determined from Gaussian fits of the ADCP current velocity (Appendix A).

A total of 97 conductivity-temperature-depth (CTD) stations were occupied during the cruise using a Seabird SBE 9/11 dual-sensor unit, with stations 2–50 in the anticyclonic eddy and stations

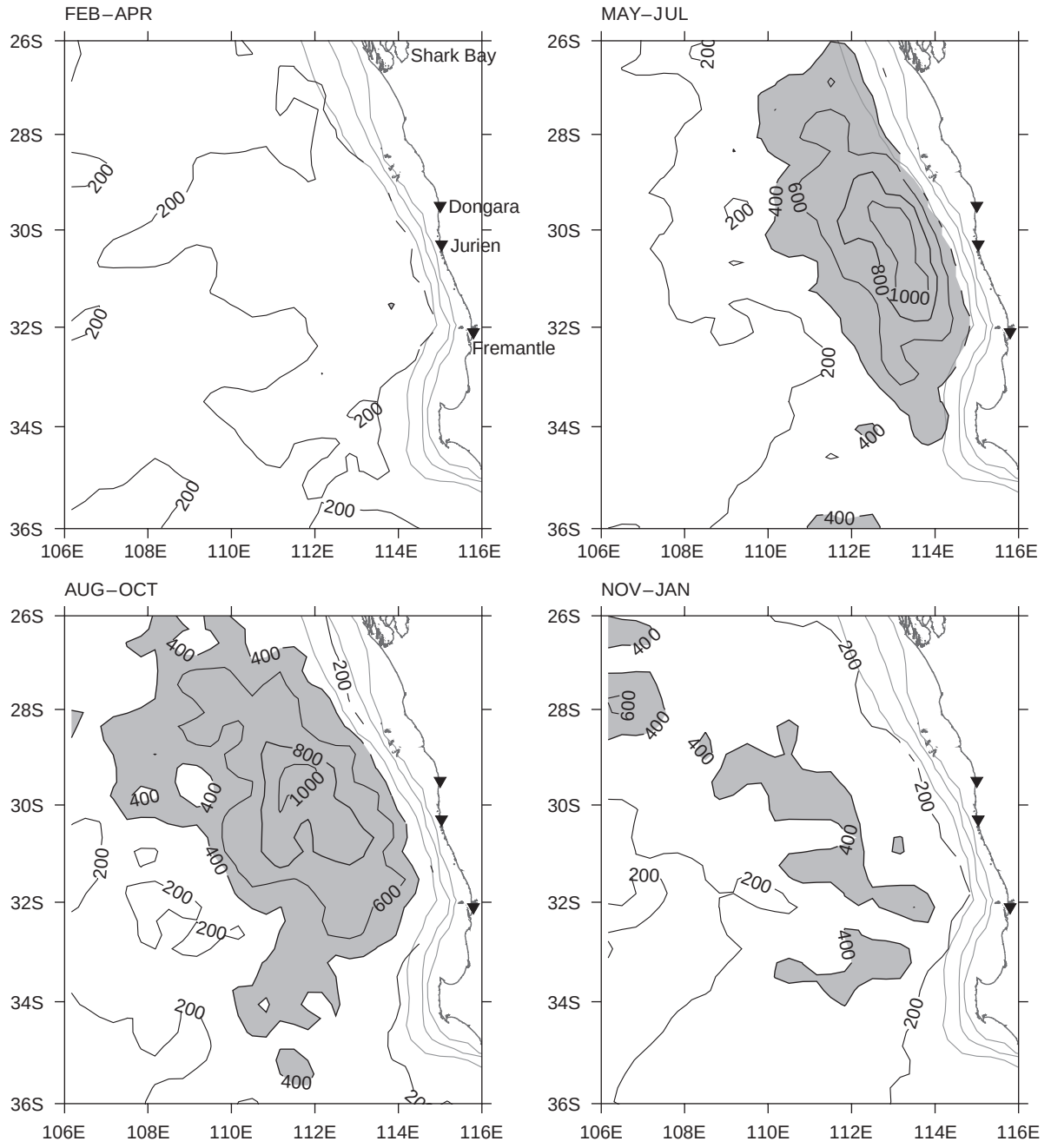

Fig. 1. Seasonally averaged sea-surface kinetic energy in the southeast Indian Ocean calculated from satellite altimeter data during 1993–2003. The unit is $cm^2 s^{-2}$ and the shaded areas denote values higher than $400\,cm^2 s^{-2}$. Since the axis of the LC is along the shelf break, which is not fully resolved by satellite altimeter, the seasonal changes shown here are mostly due to mesoscale eddies.

51–98 in the cyclonic eddy (Fig. 3). The CTD measurements were taken from the sea surface to about 500 m at most stations, measuring temperature, salinity, and fluorescence in the water column. Water samples were taken at selected CTD stations located in the centre, the body, and perimeter of the two eddies for biological research (Waite et al., 2007). The chlorophyll *a* measurements are used to calculate regression coefficients to convert CTD fluorescence measurements into chlorophyll *a* concentration. In addition, 33 Argo float temperature salinity profiles sampled in the survey domain

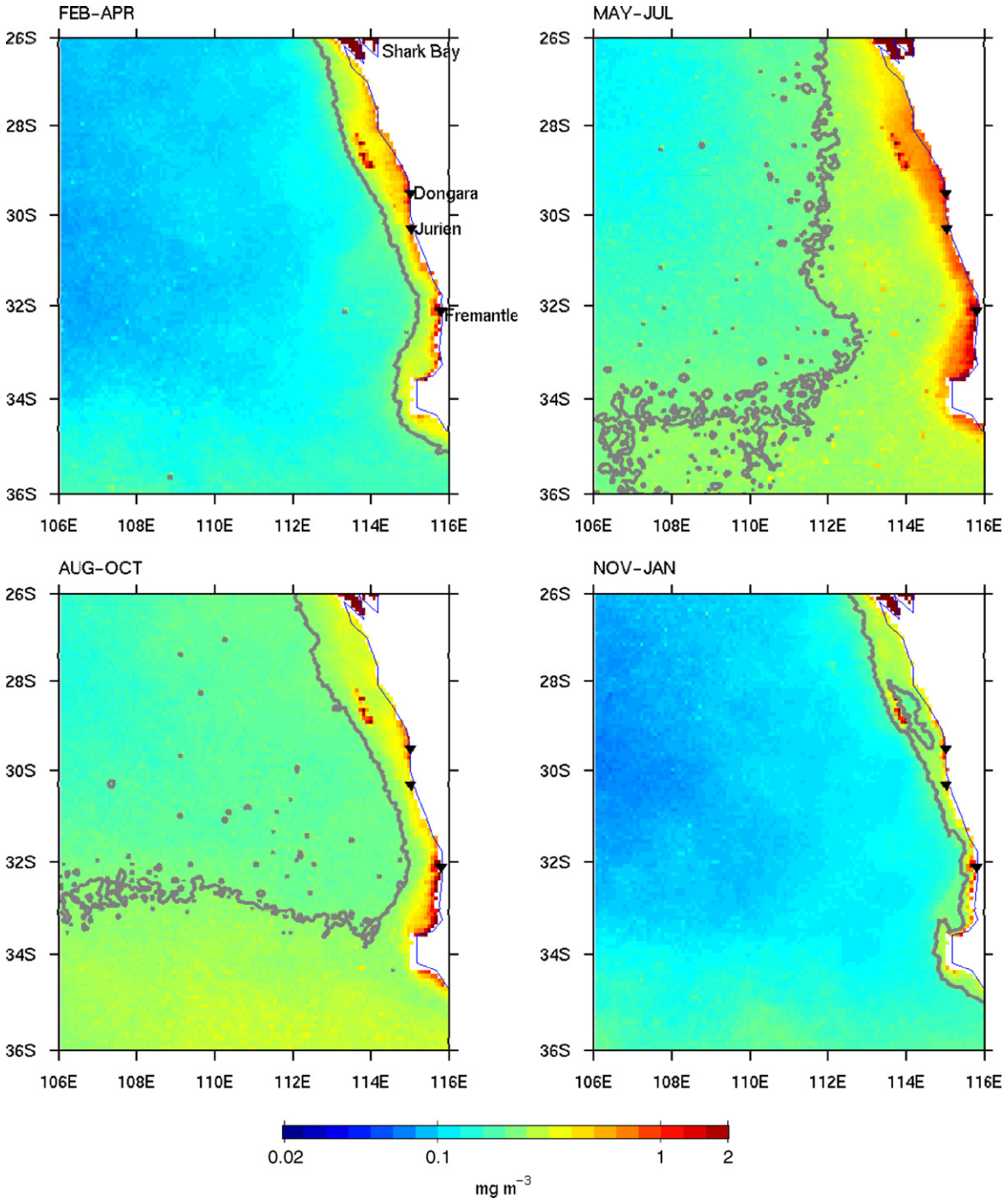

Fig. 2. Seasonally averaged SSC concentration in the southeast Indian Ocean calculated from SeaWiFS data. The unit is mg m^{-3} and the shaded lines denote the 0.2 mg m^{-3} contours.

during September–December 2003 were obtained from the International Argo Project data server. Note that one Argo float (WMO 5900262) deployed by the University of Washington was trapped within the cyclonic eddy at 1000 m for about 4 months (Fig. 3A). The Argo float data, along with the CTD data, were used to characterise the mixed-layer temperature–salinity relationship in the region. The

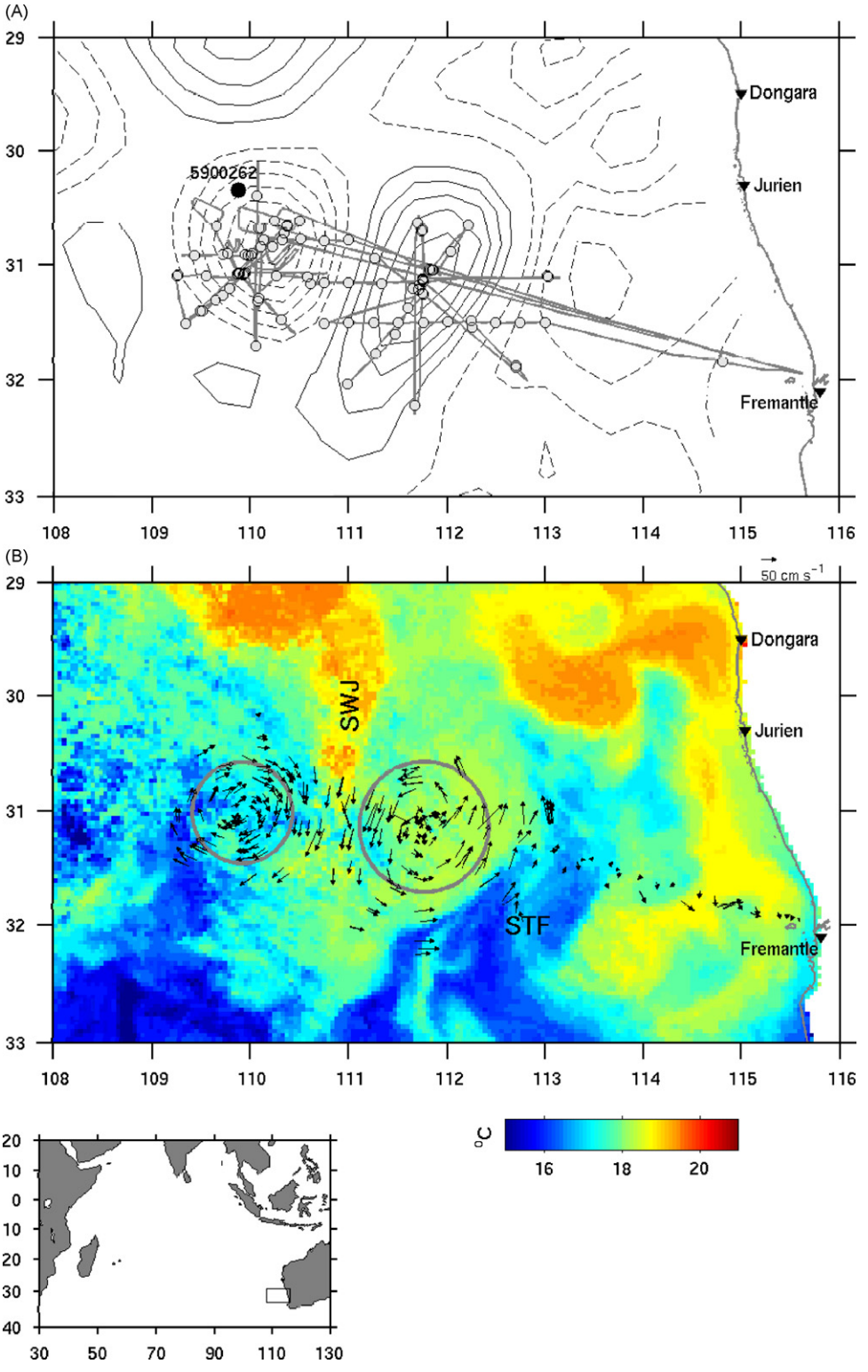

Fig. 3. (A) Sea-surface-height anomaly on 10 October 2003 off southwest WA and the cruise track of the eddy cruise (light shaded line). Solid (dashed) contours are positive (negative) anomalies at 5 cm interval from 5 (−5) cm and the zero contour is not plotted. The open circles are CTD stations during the cruise and the solid circle is the location of Argo float 5900262 on 9 October 2003. (B) Two-hourly averaged current velocity at 19 m measured from shipboard ADCP during the eddy cruise. The background shows a 3-day SST composite during the eddy cruise. SWJ and STF denote surface warm jet and subtropical front, respectively. The inset indicates the location of the survey domain in the Indian Ocean.

Table 1
Selected eddy properties determined from Gaussian fits to the shipboard data during the eddy cruise

	WC eddy	CC eddy
Centre longitude	111°46.1′E (111°37.7′E[a])	109°55.1′E (110°1.5′E)
Centre latitude	31°8.1′S (31°19.2′S)	31°0.8′S (30°56.7′S)
Eastward drift velocity ($cm\,s^{-1}$)	0.8 (−0.1)	−2.8 (−1.6)
Northward drift velocity ($cm\,s^{-1}$)	4.1 (4.6)	−1.8 (−2.6)
Peak velocity ($cm\,s^{-1}$)	65[b]	60
Height amplitude (cm)	(19)	(21)
Average radius (km)	63[b] (56)	49 (49)
Volume flux above 250 m (Sv)[c]	6.8	−4.9
Volume flux above 250 (500) m from Gradient Wind relationship (Sv)	6.8 (9.8)	−5.1 (−9.3)
Relative vorticity ζ (s^{-1})[d]	1.98×10^{-5}	-2.46×10^{-5}
ζ/f	−0.26	0.33
17.5 °C isotherm D (m)[e]	262	95
Potential vorticity $(\zeta+f)/D$ ($m^{-1}\,s^{-1}$)	-2.1×10^{-7}	-1.1×10^{-6}

[a]Numbers in parentheses are determined from altimeter sea surface height anomaly data.
[b]Averaged between 80 and 200 m.
[c]Within apparent radius.
[d]Averaged within apparent radius.
[e]A shallow isotherm used here to accommodate the ADCP measurement.

mixed-layer depth is defined with a $0.125\sigma_\theta$ increment from 10 m depth. We used air-sea flux data from the National Center for Environment Prediction (NCEP; Kalnay et al., 1996) to describe the meteorological conditions during the cruise. The shipboard surface meteorology instruments during the cruise failed to deliver useful data.

3. Evolution of the eddy pair detected from satellite data

Altimeter sea-level anomaly (Fig. 4A) shows that, on 28 May 2003, two large meander structures evolved in the LC off the southwest coast of WA, with two positive sea-surface-height anomalies (crests) centred at 30.2°S off Jurien (**A**) and at 32.6°S south of Fremantle (**B**), and a negative sea-level anomaly (trough), **C**, in between. Geostrophic current anomalies that follow the meander structures had magnitudes of 60–70 $cm\,s^{-1}$. During the following 3 months, **B** and **C** gradually pinched off from the LC and formed the two eddies in the survey domain of the October 2003 cruise (Figs. 5A and 6A). The anticyclonic structure **A** drifted northwestward, out of the domain (Fig. 6A).

Because of the proximity of **B** and **C**, they are regarded as an eddy pair or an eddy dipole structure after they detached from the LC. Hereafter they are called the warm-core (WC) and cold-core (CC) eddies due to their temperature signatures in the surface layer. The WC eddy was slightly stronger and greater in size, so that the centre of the CC eddy tended to revolve anticlockwise around the WC eddy as determined from Gaussian fits to the altimeter sea-surface-height anomaly data (Fig. 7A; Appendix A). We should be aware that this was not an isolated dipole structure, and influences from structure **A** in the north and the existence of the coastline could induce the slow northward drift of the WC eddy (Fig. 7A). The uncertainty of eddy centres determined from altimeter data will be discussed in Section 6.4.

From the Gaussian fits, both the amplitude and radius of the WC eddy decline before and during the October cruise (Fig. 7B and C). Note that the distance between the eddies and the Topex/POSEIDON satellite altimeter ground tracks may influence these numbers (Section 6.4). The CC eddy started to decay at a later stage. During the cruise, the distance between the two eddy centres is 150–180 km (Fig. 7D). From November, the two eddies start to move apart, with the CC eddy drifting southwestward and the WC eddy remaining near 30.5°S, 111°E. Morrow et al. (2004) have found that the anticyclonic and cyclonic eddies in the LC system tend to have divergent pathways when they propagate westward.

High SST is a signature of the poleward flowing LC and its meanders in satellite data (Figs. 4B–6B). There was apparent association between high SST and high SSC concentration in the meander structures (Figs. 4C–6C). Vigorous onshore–offshore

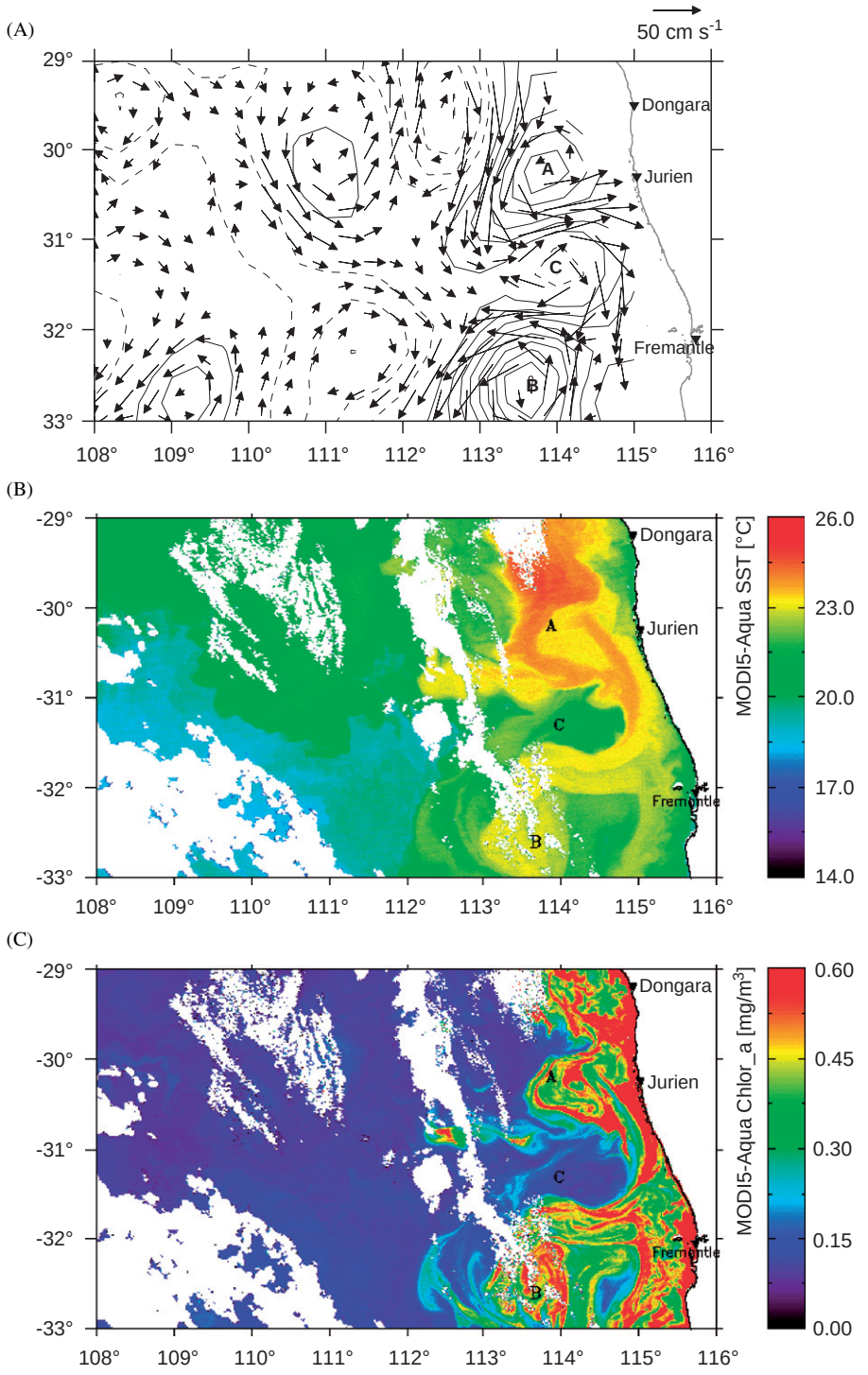

Fig. 4. (A) Sea-surface-height anomaly (same contour intervals as Fig. 1A) and surface geostrophic current anomaly (arrows) off southwest WA on 28 May 2003. (B) SST and (C) SSC concentration from MODIS satellite on 25 May 2003.

exchanges at the meander stages of the eddy formation are noted in satellite SST and SSC images. On 25 May 2003, when the LC was pushed tightly against the coast east of **C** (Fig. 4B), the LC water mixed with high SSC shelf water and was entrained into **B.** There was little SSC expression in

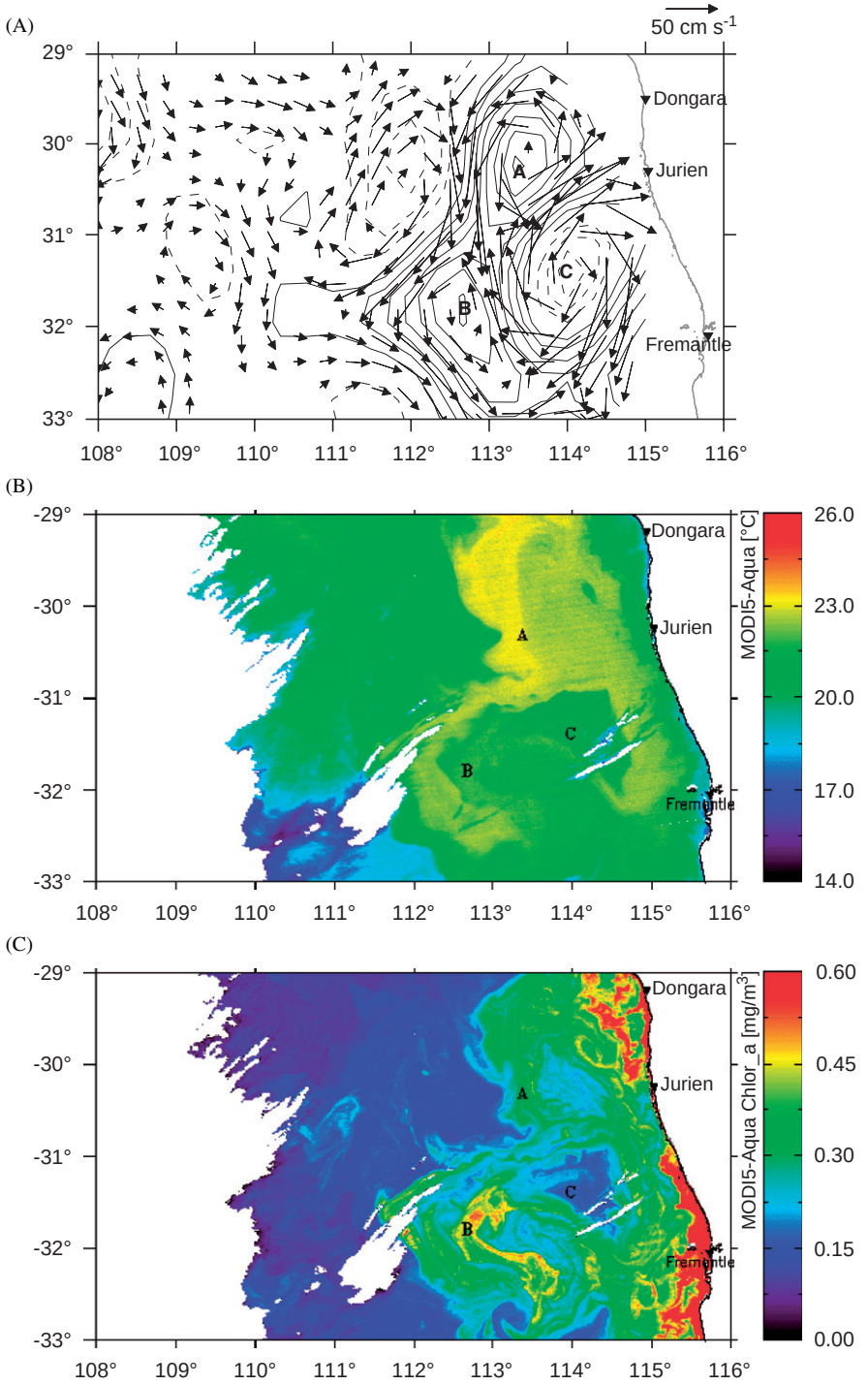

Fig. 5. Same as Fig. 4 except that the sea-surface-height and geostrophic current anomalies are on 25 June 2003, and the SST and SSC maps are from 19 June 2003.

C. In June 2003, the linkage between **B** and the shelf shifts southward, and **A** and **B** were connected by warm, high SSC water (Figs. 5B and C). In early September, the high SST and high SSC signature in the WC eddy (**B**) were maintained after the eddy detached from the current (Figs. 6B and C). In October, there was a high SST filament, a warm surface jet (WSJ), between the two eddies (Fig. 3B).

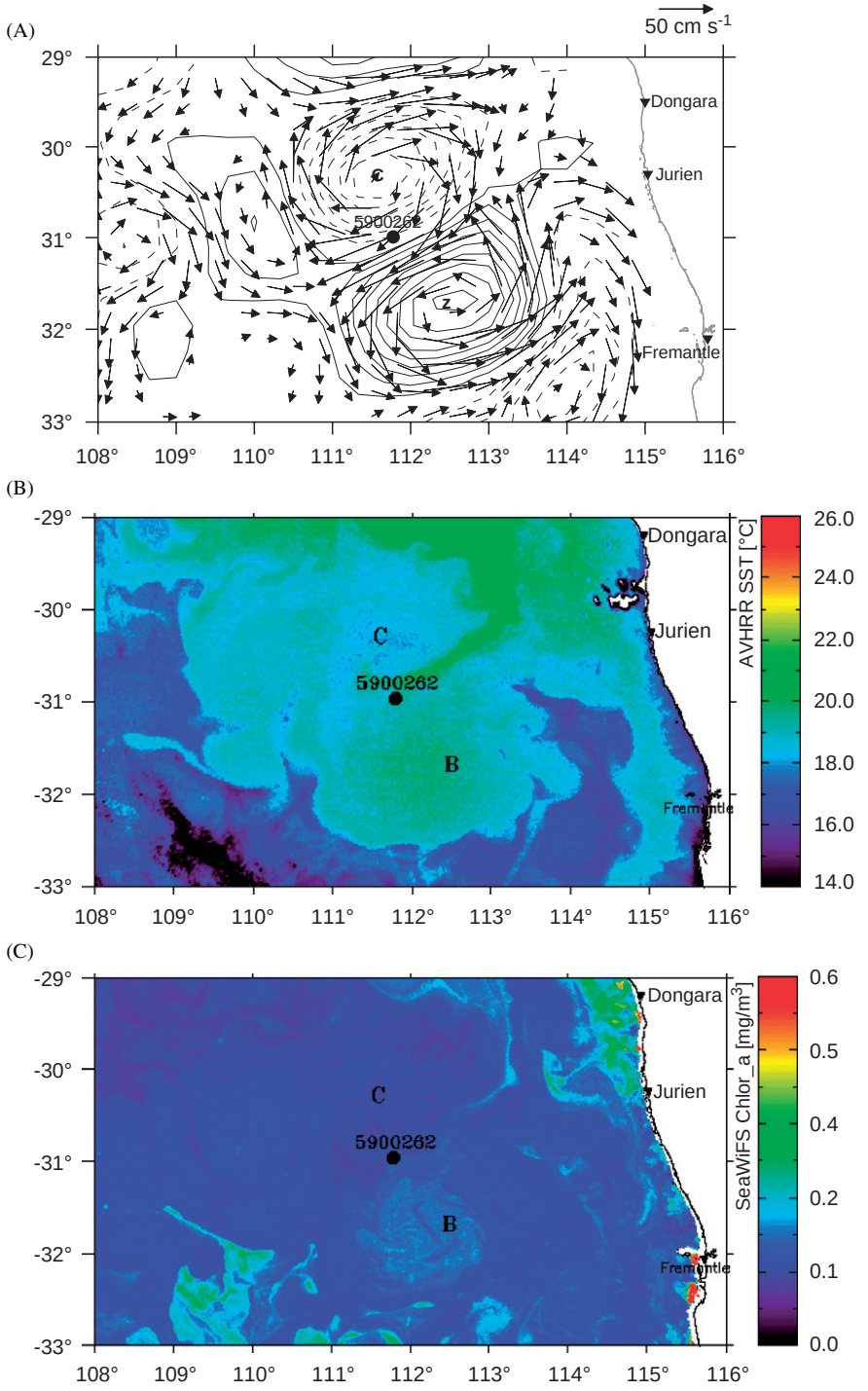

Fig. 6. Same as Fig. 4, except that all the data are from 2 September 2003, and the SST is from AVHRR and the SSC concentration is from SeaWIFS.

Low SST Subtropical Front (STF) water was found to the southeast of the WC eddy. Both the WSJ and STF water had relatively high productivity thus in addition to onshore–offshore exchanges, eddy–eddy interaction and eddy-front interaction may also be important for ocean production in the region.

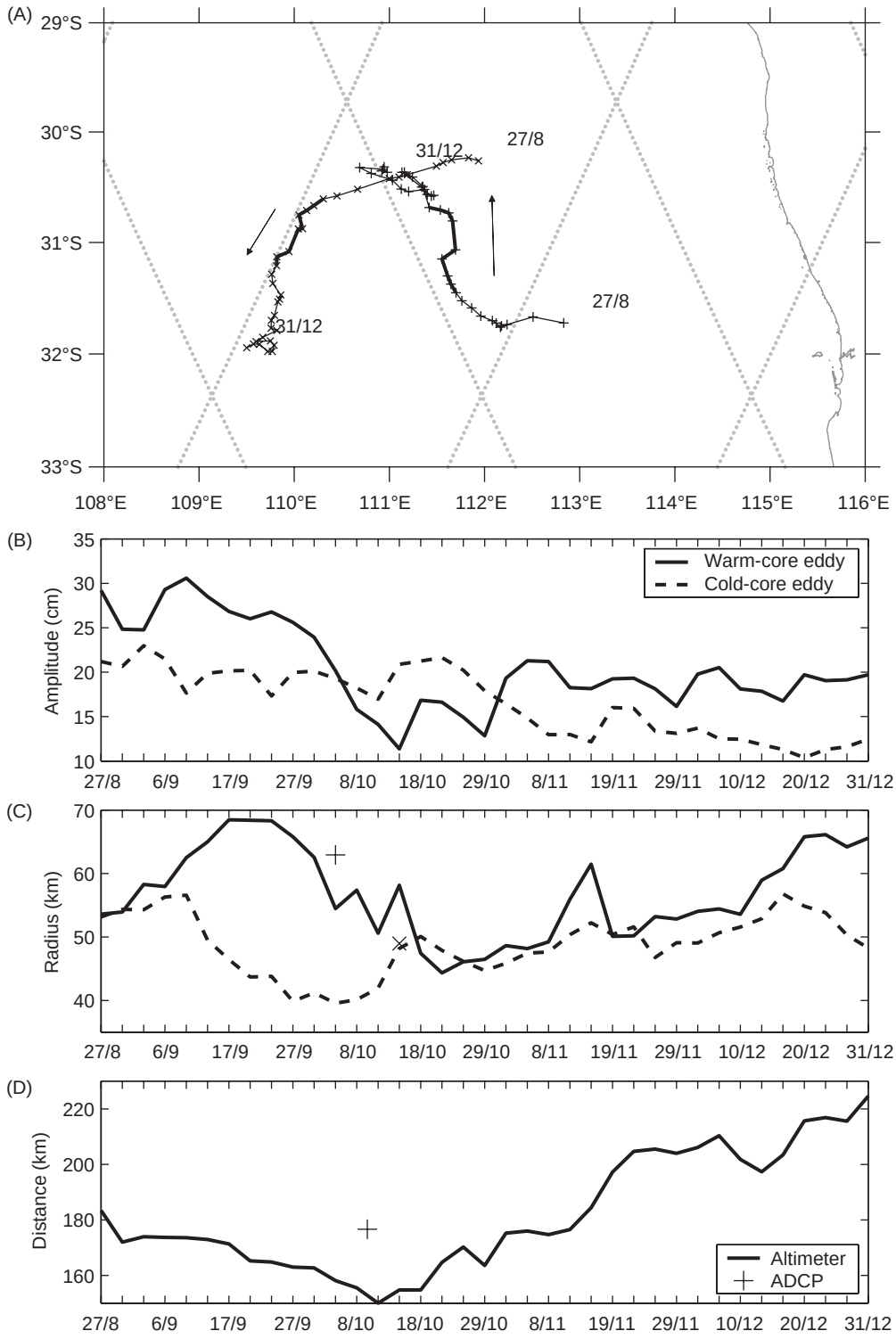

Fig. 7. (A) Lagrangian tracks of the centres of the WC eddy (plus) and the CC eddy (cross), (B) amplitudes, (C) radius, and (D) distance between the two eddy centres from the Gaussian fits. In (A), the shaded dots denote ground tracks of the T/P (Jason-1) altimeter satellite, and the solid arrows denote the drifting directions of the two eddies. In (C), the cross and plus symbols denote the mean radius determined from the ADCP data, and in (D) the cross denotes the distance between the two eddy centres determined from the ADCP data.

4. Eddy structures from shipboard observations

Gaussian shapes were fitted to the shipboard ADCP velocity data within successive 4-day windows during the survey periods of the WC and CC eddies, respectively (Appendix A). A 4-day selection was due to the fact that there are usually two sections across the eddies in 4 days so that the 2-dimensional structures of the eddies can be determined. From a tidal model output, the magnitude of the barotropic tide in the survey region is less than $2\,cm\,s^{-1}$ (Egbert and Erofeeva, 2002), and the baroclinic tide is also weak. To avoid the influence of inertial oscillations in the surface Ekman layer, fitting results below 80 m was used to determine the positions of the eddy centres. The averages of the fitting parameters over all the 4-day windows were used to determine the mean structures of the two eddies (Table 1). The residual of the Gaussian fittings are generally $5–10\,cm\,s^{-1}$ (not shown).

The WC eddy had a stronger baroclinic current structure compared with the CC eddy (Fig. 8). The apparent radius (radius where the azimuthal velocity peaks) of the WC eddy decreased from 72 km near the sea surface to about 62 km at 200 m depth, while the apparent radius of the CC eddy increased from about 44 km at the sea surface to 52 km near 250 m (Fig. 8). The peak azimuthal velocity of the WC eddy decreased from $75\,cm\,s^{-1}$ at 19 m to about $46\,cm\,s^{-1}$ at 250 m, while the peak azimuthal velocity of the CC eddy was almost constant with depth at around $60\,cm\,s^{-1}$. Thus the WC eddy was greater in size and possessed a larger integrated volume transport than the CC eddy in the surface layer (Table 1), as also seen in the satellite data (Figs. 4–6).

Isotherms in the WC eddy shows a similar bowl shape below the surface mixed layer, consistent with its baroclinic current structure (Fig. 9A). East of the WC eddy, there was a sharp temperature front due to the intrusion of the low-temperature STF from the south (see also Figs. 3B and 6B). Within the CC eddy, the isotherms displayed different shapes above and below 250 m (Fig. 9B), which tends to support a weak subsurface core and weak vertical shear in the eddy (Fig. 8B). The isothermal doming at the centre of the CC eddy did not reach the surface euphotic zone, so that there was no active upwelling at the core of the CC eddy. There was strong stratification and weak current shear (high Richardson number and low turbulent mixing) below the mixed layer of the CC eddy and hence the isothermal doming within the eddy might not have caused strong mixing across the base of the mixed layer.

The fitted eddy centres in successive 4-day windows also were used to determine the average drift speeds of the two eddies (Table 1). The average drift speeds of the eddy centres during the cruise period ($4.2\,cm\,s^{-1}$ to the north and $3.3\,cm\,s^{-1}$ to the southwest, respectively, for WC and CC eddies) are similar to those derived from the altimeter data (Table 1), although there are offsets between the eddy centres determined by the two datasets as discussed in Section 6. This provides us with confidence to assign each CTD cast with a radial distance from the moving centres of the two eddies (determined from the ADCP data). The temperature

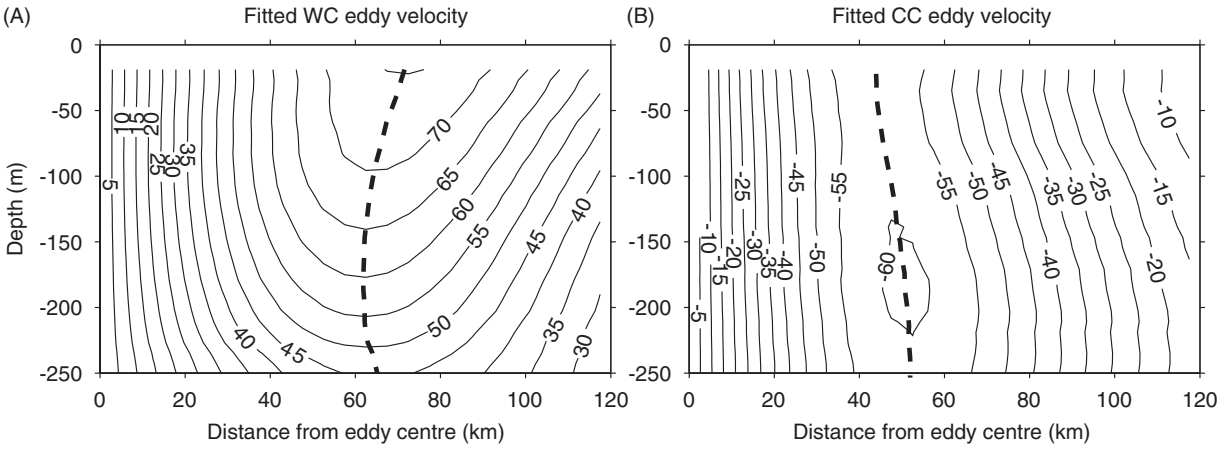

Fig. 8. Mean azimuthal velocity structures in (A) the WC eddy and (B) CC eddy from Gaussian fits to the ADCP data. The unit is $cm\,s^{-1}$, and the dashed lines denote the apparent radius.

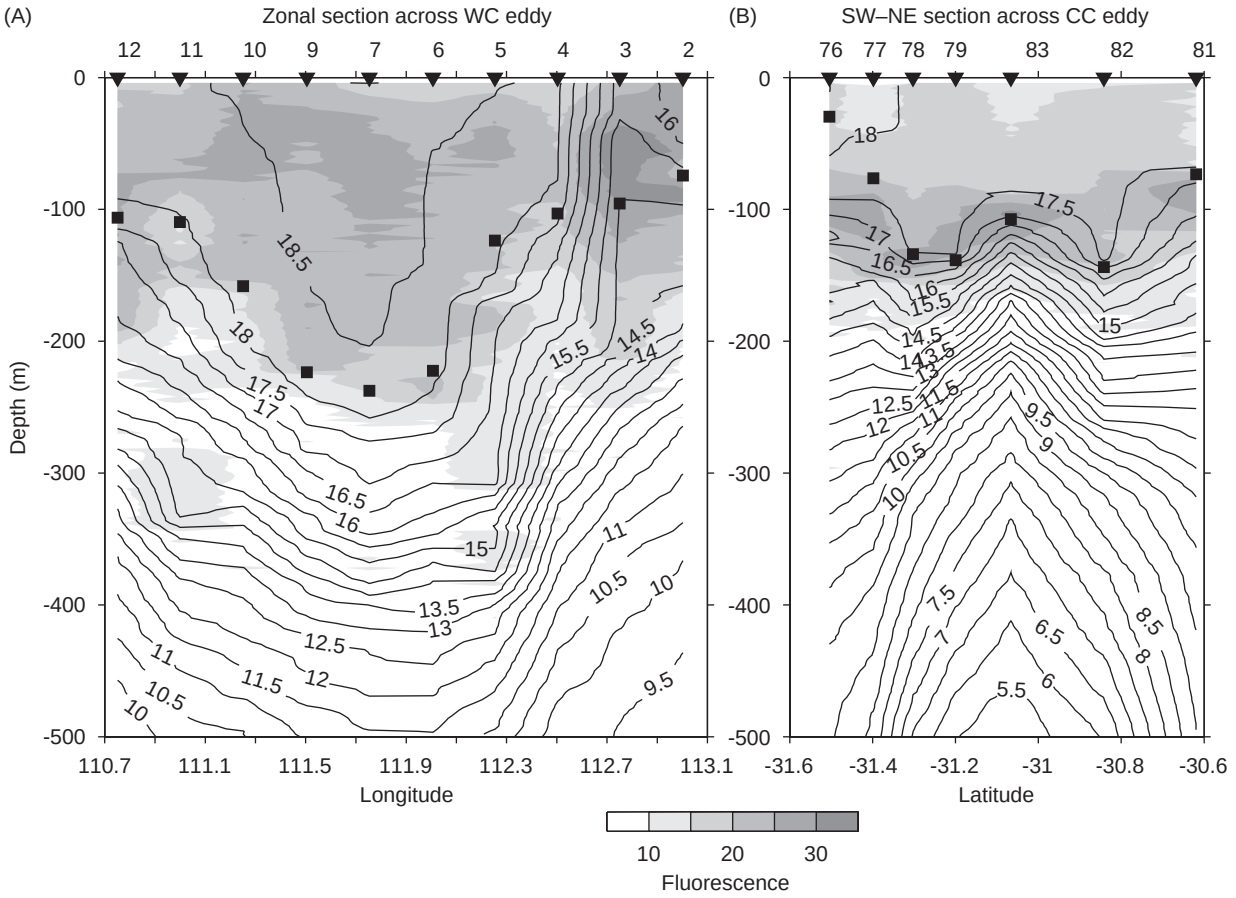

Fig. 9. Vertical temperature structures along two transects across the WC eddy (A) and the CC eddy (B). The shadings denote the fluorescence measurements and the solid squares denote the depth of the mixed layer. The station numbers of the CTD casts are denoted on the tops of the panels.

structure of each eddy is determined by fitting the temperature data at each depth with a second-order polynomial function of the radial distance. The salinity structures are simply calculated from a mean temperature–salinity relationship for each eddy. A Gaussian fit is not appropriate here due to data distribution.

Based on fitted temperature and salinity, the azimuthal geostrophic velocities of the two eddies are calculated with reference to adjusted ADCP velocity at 250 m using Eq.(B1) (Appendix B) and then the velocities are adjusted for the gradient wind relation using Eq.(B2) (Figs. 10 and 11). The centrifugal terms contribute 20–30% of the total velocity at the apparent radius, consistent with the ratio between relative (ζ) and planetary (f) vorticities (Table 1). There is a good match (less than 10% difference) between the vertical and horizontal structures of the WC eddy determined from the ADCP and gradient wind relationship (Fig. 10), while the gradient wind relationship overestimates the azimuthal velocity near the surface by almost $10\,\mathrm{cm\,s^{-1}}$ in the upper 100 m of the CC eddy (Fig. 11), which is likely due to errors in the data fittings.

In summary, the WC eddy was larger and stronger than the CC eddy in the surface layer. The two eddies had different vertical structures; WC had stronger vertical shear above 250 m and a less-stratified thermocline below the mixed layer, while the CC eddy had a more barotropic structure in the upper 250 m. Nonlinear terms are not negligible in the gradient wind relationship describing the azimuthal velocity of the two eddies, and there was no active upwelling at the centre of the CC eddy.

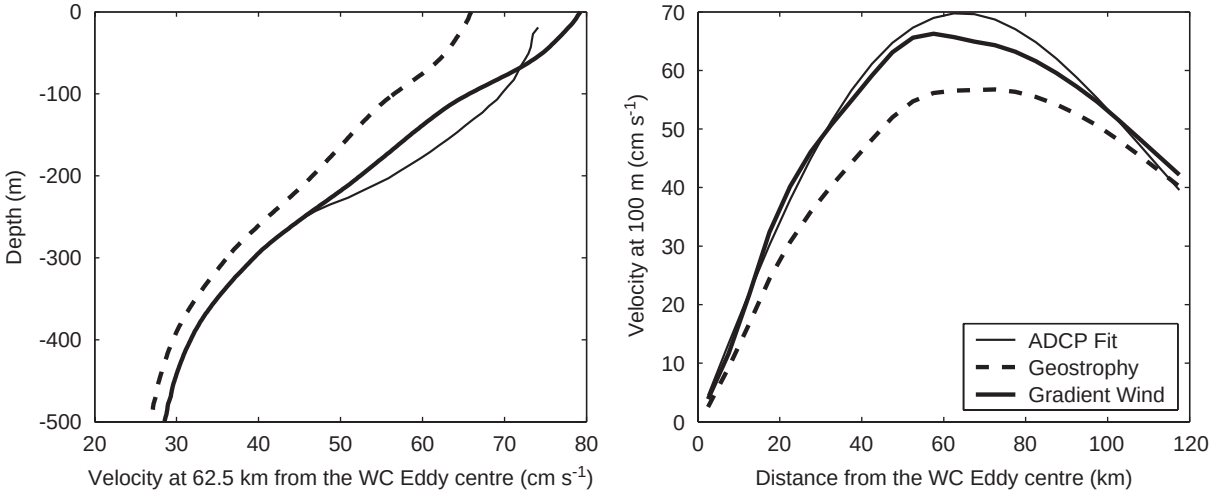

Fig. 10. The vertical (left panel) and radial (right panel) profiles of azimuthal velocity of the WC eddy, estimated from ADCP data fit, geostrophic calculation referenced to 250 m ADCP data, and the gradient wind relationship.

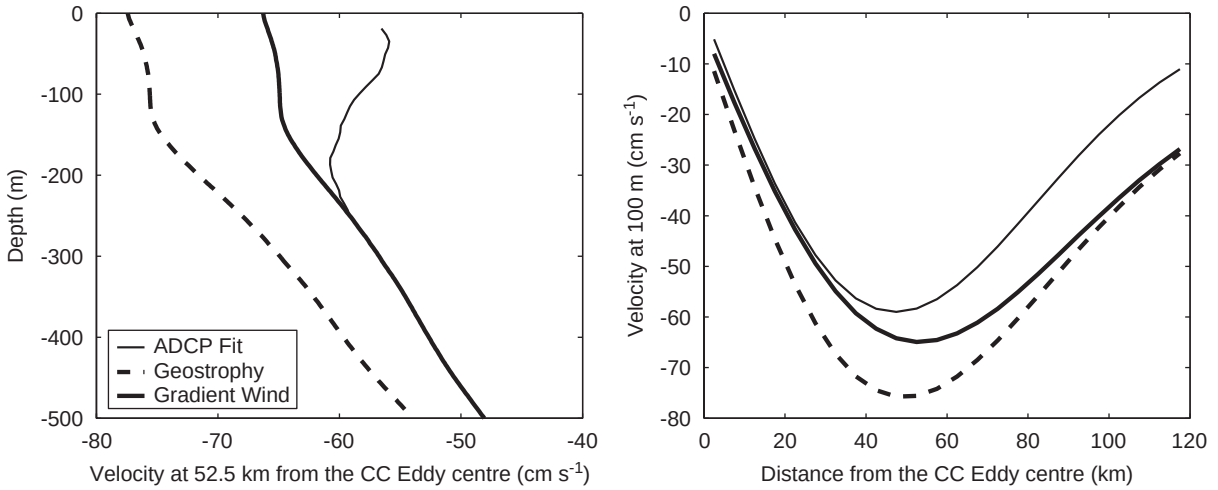

Fig. 11. The vertical (left panel) and radial (right panel) profiles of azimuthal velocity of the CC eddy, estimated from ADCP data fit, geostrophic calculation referenced to 250 m ADCP data, and the gradient wind relationship.

5. Water mass and biomass characteristics

The mixed-layer depth was over 250 m deep at the centre of the WC eddy, reduced to about 100 m at the perimeter of the eddy (Figs. 9A and 12). The mixed-layer depth was a minimum at the centre of the CC eddy, of around 100 m, and a maximum of about 140 m at 20–40 km from the eddy centre (Fig. 12).

The LC water possesses high-temperature/low-salinity characteristics in the north, and gradually becomes colder and saltier when the current flows southward, due to surface heat and freshwater losses, and also due to mixing with ambient subtropical waters. On the other hand, the subtropical surface water has its salinity maximum character at about 32°S. From a *T–S* diagram of the mixed-layer water, the WC eddy contained mainly LC water, while the CC eddy contained mainly high-salinity open-ocean subtropical water (Fig. 13). The *T–S* properties within the eddies are rather stable during the course of the cruise, which is on the one hand due to the deep mixed-layer depth and, on the other hand, due to the very moderate heat and freshwater losses at the air–sea interface (Fig. 14). While the air–sea fluxes may modify the water properties very slowly, they may be important in the vertical mixing to maintain the biomass in the

mixed layer of the WC eddy (Thompson et al., 2007; Greenwood et al., 2007). Note that the nitrate was depleted in the mixed layer of both eddies and there is lower concentration of silicate in the WC eddy (Thompson et al., 2007).

The low vorticity at the centre of the WC eddy manifests the low-latitude origin of its source water (Table 1). Assuming conservation of vorticity ($f+\zeta$) with f and ζ taken from Table 1, the water in the WC eddy could be tracked upstream in the LC to 22–23°S, the origin of the LC, if the source water initially has no relative vorticity. Note that the poleward flowing LC waters acquired positive relative vorticity in order to conserve its total vorticity. The total volume of the WC eddy in the upper 450 m, which is the depth of the vertical extent of the LC water as determined from the depth of the 11.5 °C isotherm (Feng et al., 2003), is $5.6\times10^{12}\,m^3$. A heat content anomaly of the WC eddy referenced to the temperature profile outside the perimeter of the eddy, 0.45×10^{20} J, is obtained from the fitted temperature field in the upper 300 m.

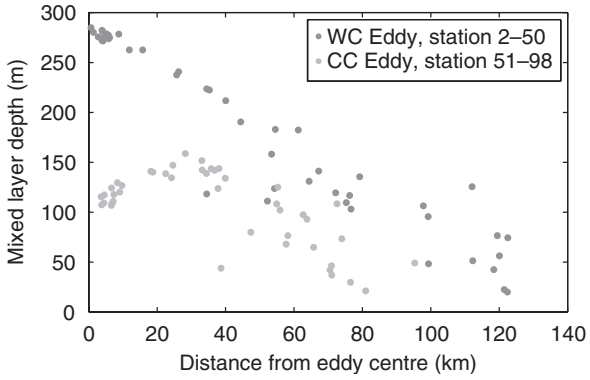

Fig. 12. Mixed-layer depths (estimated from the CTD data) as a function of distance from eddy centres.

From shipboard measurement across the two eddies, high fluorescence was observed in the surface mixed layer in the WC eddy, with the maximum at the mid-depth of the mixed layer (Fig. 9A). This is in contrast with the CC eddy, where the fluorescence maximum was near the base of the mixed layer, forming a deep chlorophyll maximum (Fig. 9B). The fluorescence structure is consistent with the chlorophyll *a* measurements during the cruise, and a linear relationship between chlorophyll *a* concentration and fluorescence can be established when fluorescence readings are above 13 relative scale (Fig. 15A).

The chlorophyll *a* biomass within the two eddies was estimated using the satellite ocean colour data (Appendix C) and the relationship between fluorescence and chlorophyll *a* concentration

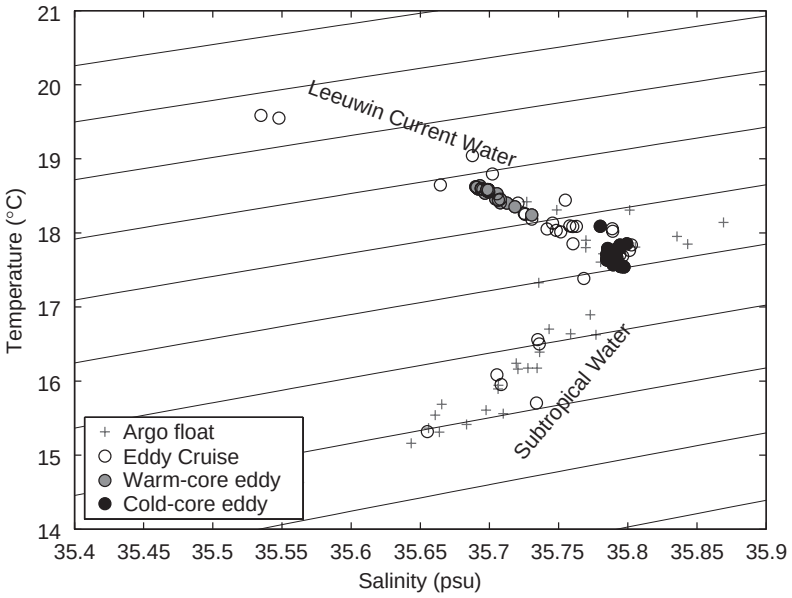

Fig. 13. Mixed-layer temperature–salinity relationship estimated from the CTD data during the October 2003 cruise and Argo float data during the same season. The filled grey and black dots denote water masses within the cores of the WC and CC eddies, which are the LC water and subtropical water, respectively.

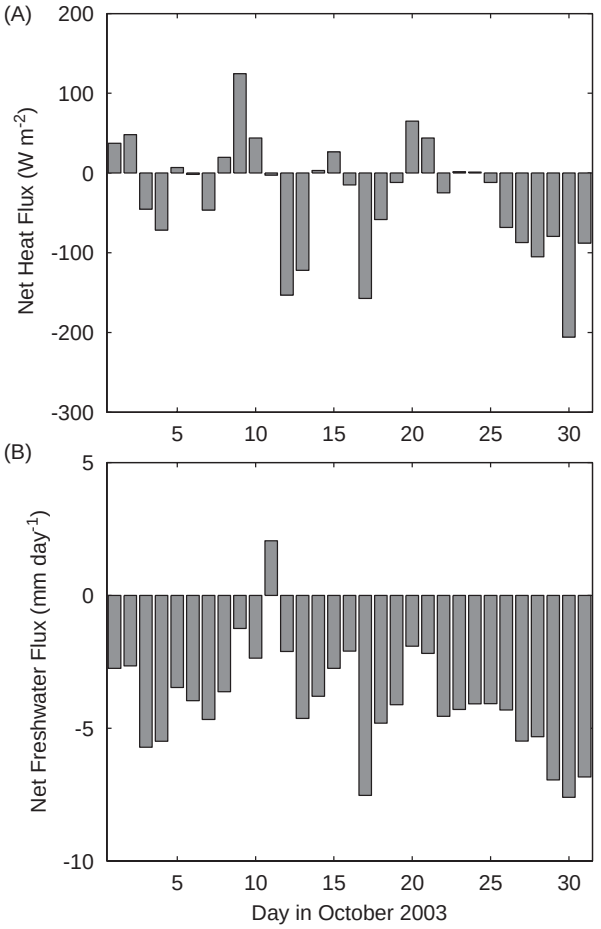

Fig. 14. Daily average of net air–sea (A) heat and (B) freshwater fluxes from NCEP reanalysis during October 2003. Positive values denote net heat and freshwater inputs into the ocean across the air–sea interface.

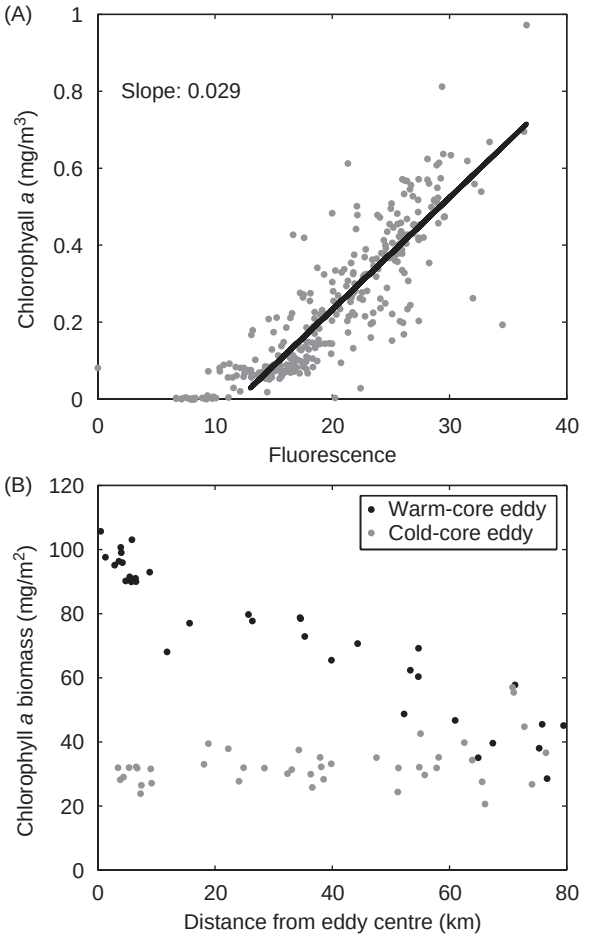

Fig. 15. (A) Relationship between chlorophyll *a* concentration and the fluorescence within the two eddies. The solid line shows a linear regression between the two variables for data points with fluorescence readings higher than 13 (relative scale). (B) Radial distribution of the 0–300 m integrated chlorophyll *a* biomass, estimated with the regression between chlorophyll *a* concentration and fluorescence.

(Fig. 15B). From fluorescence data, there was a high concentration of chlorophyll *a* biomass at the centre of the WC eddy ($\sim$100 mg m^{-2} in the upper 300 m), which gradually decreased toward the eddy perimeter and droped to background values of $\sim$40 mg m^{-2} beyond the eddy radius. The biomass in the CC eddy tended to be slightly less than that near its perimeter. The biomass in the euphotic zone estimated from the satellite ocean-colour data (using cloud free images before and after the cruise) tend to agree with the 0–100 m integrated biomass in both eddies (Table 2). The weak temporal variation of the biomass from the satellite estimates during the cruise period is consistent with the almost balanced production and grazing rates of phytoplankton within the two eddies (Paterson et al., 2007).

Averaged within the eddy radius, the chlorophyll *a* biomass in the WC eddy was almost twice of that in the CC eddy, as estimated from both the fluorescence and satellite data (Table 2). Thus, as indicated by the satellite SSC concentration, the CC eddy in this region was not associated with increased chlorophyll *a* values. The WC eddy is estimated to have had more than 3×10^8 g chlorophyll *a* biomass in the euphotic zone and more than 7×10^8 g in the upper 300 m (Table 2). The Subtropical front water east of the WC eddy also tended to have high fluorescence values (Fig. 9A).

Table 2
Chlorophyll *a* biomass in the upper 100 and 300 m within the eddy apparent radii

	Date	Average biomass (mg chlorophyll $a\,m^{-2}$)			Total biomass (10^8 g chlorophyll *a*)		
		Satellite Z_{eu}	Fluor. 100 m	Fluor. 300 m	Satellite Z_{eu}	Fluor. 100 m	Fluor. 300 m
WC eddy	May 25	42	–	–	5.2	–	–
	Jun. 19	34	–	–	4.3	–	–
	Aug. 28	30	–	–	3.8	–	–
	Sep. 2	30	–	–	3.8	–	–
	Cruise	–	31	59	–	3.8	7.4
	Nov. 8	26	–	–	3.2	–	–
CC eddy	May 25	20	–	–	1.5	–	–
	Jun. 19	30	–	–	2.3	–	–
	Aug. 28	16	–	–	1.2	–	–
	Sep. 2	17	–	–	1.3	–	–
	Cruise	–	17	31	–	1.3	2.4
	Nov. 8	13	–	–	1.0	–	–

The satellite estimates are based on statistical relationships that have been validated in this region (Appendix C). The euphotic zone (Z_{eu}) is estimated to be between 80 and 120 m.

Table 3
Characteristics of anticyclonic eddies off eastern boundaries

	Formation latitude range	Maximum amplitude (cm)	Diameter (km)	Life span (years)
Agulhas	39°S	50	200–500	Up to 4
HAIDA	51–60°N	40	150–300	>2
Iberian	39–42°N	15	30–70	Up to 1
LC	28–32°S	>60	100–400	<2

6. Discussion and summary

6.1. Comparison with other eastern boundary eddies

All other eastern boundary eddies in comparison are generated at higher latitudes than the LC eddies (Table 3). The HAIDA eddy in the Gulf of Alaska and Agulhas ring off the Benguela Current in the southeast Atlantic are both anticyclonic and have multi-year life spans (Miller et al., 2005; Crawford et al., 2005; Garnier et al., 2003). Those eddies have spatial scales comparable with the LC anticyclonic eddies; however weaker in sea level anomaly amplitudes. Note that at higher latitudes, the same sea-level anomaly corresponds to weaker geostrophic current due to reduced Coriolis coefficient. The anticyclonic eddies in the Iberian Poleward Current are much smaller and weaker (Oliveira et al., 2003; Peliz et al., 2005).

The HAIDA eddies are formed from the merging of small anticyclonic eddies due to buoyant plumes from a strait. The Agulhas rings are produced by the eddy shedding process of the Agulhas Retroflection system. Both mechanisms generate dominantly anticyclonic vorticities so that only anticyclonic eddies are observed in these two systems. Peliz et al. (2003) proposed a cyclogenesis mechanism due to the instability of the oppositely-flowing undercurrent to explain the presence of anticyclonic–cyclonic eddy pairs in the Iberian Poleward Current system. Rennie et al. (2007) has suggested that a similar mechanism could produce cyclonic eddies in the LC system due to the existence of the Leeuwin Undercurrent.

The short life span of the LC anticyclonic eddies compared to the HAIDA and Agulhas eddies, despite its stronger magnitude, is likely due to the rugged bottom bathymetry off the coast of WA. Thus, unlike the other two systems where the anticyclonic eddies can affect the heat balance or biogeochemical processes across the basin, the influence of the LC eddies is within a few hundred kilometres off the coast.

6.2. Physical processes affecting the ocean production

There is a good association between high SST, which is an indicator of the LC water, and high SSC from the analysis of the satellite data (Figs. 4–6). The WC eddy gains its high surface chlorophyll *a* biomass during eddy formation, which is a distinct feature from other eastern boundary systems (e.g., Mizobata et al., 2002; Hormazabal et al., 2004; Crawford et al., 2005), likely due to different physical dynamics. This process was not sampled by the October 2003 cruise when the eddy pair was at the mature stage. Here we discuss two physical processes that are likely important for biological productivity during the eddy formation.

The first process is the interaction between the meandering boundary current and the continental shelf topography. Upstream of a cyclonic meander, the current crosses isobaths into the shelf, while downstream of a cyclonic meander the current is directed offshore into deep water. Vertical motions are induced when the boundary current flows across isobaths (Osgood et al., 1987), which may be a mechanism for bringing nutrients to the euphotic zone from the nutricline. Alternatively, when the current is in close contact with the shelf inshore of a cyclonic meander, the coastal waters with higher surface chlorophyll *a* may be entrained from the shelf into the LC. Again the present dataset does not allow us to understand the detailed processes that have been involved. A one-dimensional numerical simulation suggests that the initial injection of high nutrient/biomass water into a WC eddy is crucial in generating the sustained high biomass during its life cycle (Greenwood et al., 2007).

The second effect is vertical mixing within the LC. The LC is a poleward flowing warm current and it undergoes significant heat loss at the air–sea interface along its meandering course. The surface heat loss can cause convective mixing in the surface layer that erodes the thermocline as well as the nutricline within and immediately below the current. The strong shear between the LC and the underlying water also may enhance vertical mixing, which brings nutrients into the euphotic zone and drives primary production. Better in situ measurements and numerical models are necessary to quantify the role of vertical mixing during the eddy evolution.

By assuming symmetry, this study only provides a zero-order description of the two eddies after their mature stage. Upwelling at the centre of the WC eddy due to its frictional decay may enhance the nitrate uptake and phytoplankton biomass (Flierl and Mied, 1985; Franks et al., 1986; Nelson et al., 1989). Kinetic effect may lift high-nitrate water parcels vertically into the euphotic zone when the CC eddy revolves around the WC eddy (Flierl and Davis, 1993), which can cause the higher phytoplankton biomass near the edge of the CC eddy. Instability of the eddies and forcing by the surface winds also can produce vertical circulation within the eddies that drive ocean production (Martin and Richards, 2001). These processes may be important, but they cannot be resolved from the current survey data. Numerical simulations are necessary to tackle these questions.

6.3. Offshore heat and biomass transports

Part of the high biomass water entrained in LC is transported offshore, mainly by the WC eddies. Here we estimate the magnitude of the offshore biomass transport due to eddy activities based on the eddy cruise data. Note that the WC eddy sampled during the cruise is larger than the typical size of anticyclonic eddies measured by Morrow et al. (2003) (Waite et al., 2006). If we match the heat fluxes with Morrow et al. (2003) and Feng et al. (2005), three eddies of the same size as the WC eddy can transport 0.004 PW (10^{15} W) of heat offshore off the southwest WA. Note that three eddies could also carry offshore nearly 20% of the annual mean volume transport (3.4 Sv) of the LC at 32°S (Feng et al., 2003).

When we use the average chlorophyll *a* concentration in the CC eddy as typical for the open-ocean water, the anomalous biomass contained in WC eddy is about 3.5×10^8 g chlorophyll *a*. This is only a crude estimate because we neglect all the biogeochemical processes during the eddy evolution. If three similar size WC eddies are formed and propagated offshore each year, the total offshore transport of chlorophyll *a* biomass is about 1×10^9 g. Or it is equivalent to about $4–5 \times 10^{10}$ g C year^{-1} of carbon export from the shelf to open ocean, when using a fixed, conservative carbon to chlorophyll *a* ratio of 40–50. This may be an underestimate of the total offshore transport, because there seems to be significant biomass reduction between May and August (Figs. 4–6). Also short-lived eddy activity is quite important in the onshore–offshore exchange processes near the shelf break (Domingues et al., 2006).

Although this offshore flux of phytoplankton biomass may be small compared to those from other upwelling coasts (e.g., Thomas et al., 2004), the enhanced biomass in the offshore region still may be important to pelagic fisheries and fisheries recruitments in the southeast Indian Ocean. For example, the western rock lobster (*Panulirus cygnus*), Australia's largest single species fishery by value, spends a long larvae stage in the offshore region (Phillips, 1981; Griffin et al., 2001).

6.4. Accuracy of eddy centres determined from altimeter data

The shipboard ADCP data provide a good opportunity to accurately capture the movement of eddy centres, and it also could provide a ground truth for the eddy centres determined from satellite altimeter data.

During the eddy cruise, the centre of CC eddy was very close to a Topex/POSEIDON (Jason-1) ground track (Fig. 7A), so that the centre of the CC eddy determined from the altimeter data was only about 13 km from that determined from the ADCP data. By contrast, the WC eddy was away from the ground tracks during the cruise (Fig. 7A), so that the eddy centre estimated from the altimeter data was about 25 km from the ADCP estimate (Table 1). The drop of sea-level anomaly in the WC in October (Fig. 7B) may also be partly related to the movement of the eddy away from the satellite altimeter ground track. From the ADCP estimate, the average distance between the eddy centres was 177 km, which is underestimated by 24 km in the altimeter data (Fig. 7D).

6.5. Summary

In this study, we have used satellite data and shipboard data to track the temporal evolution of two adjacent counter-rotating mesoscale eddies that formed from LC meanders off the southwest coast of WA during 2003. The spatial structures of the two eddies were elucidated by fitting satellite and shipboard data with Gaussian eddy structures. Both eddies reached their mature stages during the eddy cruise. The WC had stronger vertical shear above 250 m and a less stratified thermocline below the mixed layer, while the CC eddy had a more barotropic structure in the upper 250 m. There was no active upwelling at the centre of the CC eddy during the eddy cruise. The physical characterisation of the two eddies set the scene for interpretation of the biogeochemical measurements during the cruise.

By vorticity conservation, the LC water mainly feeds into the WC eddy, as confirmed by the mixed-layer temperature–salinity relationship. The WC eddy had a deeper mixed layer, which consists of the warm, low-salinity LC water with high chlorophyll *a* biomass, while the CC eddy had lower phytoplankton biomass, mostly within a deep chlorophyll maximum below its mixed-layer depth.

We have suggested two processes that may enhance the phytoplankton biomass within the LC waters and then within the WC eddy: vertical mixing and interaction between the meandering current and shelf topography. The vertical mixing can be caused either by surface heat loss or vertical shear of the current, while the interaction with the shelf topography may cause localized upwelling or entrainment of productive water from the shelf. Further cruises have been proposed to investigate these hypotheses. The offshore biomass transport by the WC eddies is a significant portion of austral summer to winter increase of the chlorophyll *a* biomass in the offshore region and could be important for fisheries recruitment off WA.

Acknowledgements

This work was supported by the Strategic Research Fund for Marine Environment. We thank all the colleagues who participated in the Eddies cruise (SS08/2003) as well as the officers and crew of the R.V. *Southern Surveyor* for assistance in the collection of field data. We acknowledge the MODIS Oceans Project (NASA GSFC) and the SeaWiFS Project (NASA GSFC) and ORBIMAGE for MODIS and SeaWiFS data products. AVHRR imagery was provided by Western Australian Satellite Technology and Application Consortium (WASTAC). We thank Peter Craig and Tony Koslow for valuable comments.

Appendix A. Gaussian fits to sea surface height anomaly and ADCP current

To determine the centres and structures of the mesoscale eddies, we fit the altimeter sea-surface-height anomaly, h, at each time frame with a Gaussian shape

$$h = h_0 \lfloor \exp\,(1 - r^2/r_0^2)/2 \rfloor, \qquad \text{(A.1)}$$

where h_0 is the amplitude of the eddy at the eddy centre, $r^2 = (x - x_0)^2 + (y - y_0)^2$ is the distance square from the data position (x, y) to the centre of the eddy (x_0, y_0), and r_0 is the radius of the eddy. This approach is adopted from Feng et al. (2001). The four variables (x_0, y_0, h_0, r_0) were determined by minimizing the residual within a $2^\circ \times 2^\circ$ box around pre-seeded eddy centre, using a nonlinear Simplex (direct search) method built in Matlab.

Similar Gaussian shape was fitted to the ADCP current velocity data at each depth within a temporal moving window

$$v = v_0(r/r_0)\exp\lfloor(1 - r^2/r_0^2)/2\rfloor, \tag{A.2}$$

where v_0 is peak azimuthal velocity at distance r_0 from the eddy centre. The variables can be determined from a similar procedure as for sea-surface-height anomaly, except that the ADCP velocity is projected onto the azimuthal direction relative to the eddy centre.

Appendix B. Gradient wind relationship

The gradient wind relationship for a symmetric eddy structure is

$$-fV_\theta = -fV_g + V_\theta^2/r, \tag{B.1}$$

where the azimuthal velocity, V_θ, is positive for an anticyclonic eddy and negative for a cyclonic eddy. Knowing the geostrophic velocity, V_g, the azimuthal velocity can be calculated as

$$V_\theta = -\tfrac{1}{2}\left(fr + \sqrt{f^2r^2 + 4frV_g}\right). \tag{B.2}$$

Appendix C. Biomass estimated from SeaWiFS imagery

Estimates of biomass within the euphotic zone ($\mathrm{Chl_{tot}}$) were obtained from the SeaWiFS chlorophyll *a* data ($\mathrm{Chl_{sat}}$) using the relationships proposed by Antoine and Morel (1996) for uniform (C1) and nonuniform (C2) biomass profiles,

$$\log_{10}(\mathrm{Chl_{tot}}) = 1.808 + 0.449X + 3.927\times10^{-2}X^2 - 8.574\times10^{-3}X^3 - 4.826\times10^{-2}X^4, \tag{C.1}$$

$$\log_{10}(\mathrm{Chl_{tot}}) = 1.774 + 0.557X - 2.915\times10^{-2}X^2 + 1.671\times10^{-2}X^3 - 2.706\times10^{-2}X^4, \tag{C.2}$$

where $X = \log_{10}(\mathrm{Chl_{sat}})$. These functions are generally appropriate for the region of interest (L. Majewski, personal communication). The total biomass within an eddy is estimated as $B_{\mathrm{tot}} = \pi\sum_i^{n-1}\mathrm{Chl_{tot}}_i(r_{i+1}^2 - r_i^2)$, where $\mathrm{Chl_{tot}}_i$ is the column biomass at radius r_i and the series of n points have been sorted by distance from the centre of the eddy.

References

Antoine, D., Morel, A., 1996. Oceanic primary production 1. Adaptation of a spectral light-photosynthesis model in view of application to satellite chlorophyll observations. Global Biogeochemical Cycles 10 (1), 43–55.

Bidigare, R.R., Benitez-Nelson, C., Leonard, C.L., Quay, P.D., Parsons, M.L., Foley, D.G., Seki, M.P., 2003. Influence of a cyclonic eddy on microheterotroph biomass and carbon export in the lee of Hawaii. Geophysical Research Letters 30 (6), 1318.

Crawford, W.R., Brickley, P.J., Peterson, T.D., Thomas, A.C., 2005. Impact of Haida eddies on chlorophyll distribution in the eastern Gulf of Alaska. Deep-Sea Research II 52, 975–989.

Cresswell, G.R., Golding, T.J., 1980. Observations of a south-flowing current in the southeastern Indian Ocean. Deep-Sea Research 27, 449–466.

Domingues, C.M., Wijffels, S.E., Maltrud, M.E., Church, J.A., Tomczak, M., 2006. The role of eddies in cooling the Leeuwin Current. Geophysical Research Letters, 2005GL025216.

Ducet, N., Le Traon, P.-Y., Reverdin, G., 2000. Global high resolution mapping of ocean circulation from TOPEX/Poseidon and ERS-1/2. Journal of Geophysical Research 105, 19477–19498.

Egbert, G.D., Erofeeva, S.Y., 2002. Efficient inverse modelling of barotropic ocean tides. Journal of Atmospheric and Oceanic Technology 19 (2), 183–204.

Falkowski, P.G., Ziemann, D., Klber, Z., Bienfang, P.K., 1991. Role of eddy pumping in enhancing primary production in the ocean. Nature 353, 55–58.

Fang, F., Morrow, R., 2003. Evolution, movement and decay of warm-core Leeuwin Current eddies. Deep-Sea Research II 50, 2245–2262.

Feng, M., Lukas, R., Hacker, P., 2001. Spinup of a submesoscale eddy in the TOGA COARE intensive flux array during the spindown of an intense eastward jet. Journal of Physical Oceanography 31 (3), 711–724.

Feng, M., Meyer, G., Pearce, A., Wijffels, S., 2003. Annual and interannual variations of the Leeuwin Current at 32°S. Journal of Geophysical Research 108 (11), 3355.

Feng, M., Wijffels, S., Godfrey, J.S., Meyers, G., 2005. Do eddies play a role in the momentum balance of the Leeuwin Current? Journal of Physical Oceanography 35 (6), 964–975.

Flierl, G.R., Davis, C.S., 1993. Biological effects of Gulf Stream meandering. Journal of Marine Research 51, 529–560.

Flierl, G.R., Mied, R.P., 1985. Frictionally-induced circulations and spin-down of a warm core ring. Journal of Geophysical Research 90 (C5), 8917–8927.

Franks, P.J.S., Wroblewski, J.S., Flierl, G.F., 1986. Prediction of phytoplankton growth in response to the frictional decay of a

warm-core ring. Journal of Geophysical Research 91 (C6), 7603–7610.

Garnier, E., Verron, J., Barnier, B., 2003. Variability of the South Atlantic upper ocean circulation: a data assimilation experiment with 5 years of TOPEX/POSEIDON altimeter observations. International Journal of Remote Sensing 24, 911–934.

Godfrey, J.S., Ridgway, K.R., 1985. The large-scale environment of the poleward-flowing Leeuwin Current, Western Australia: longshore steric height gradients, wind stresses, and geostrophic flow. Journal of Physical Oceanography 15, 481–495.

Greenwood, J., Feng, M., Waite, A., 2007. A one-dimensional simulation of biological production in two contrasting mesoscale eddies in the southeast Indian Ocean. Deep-Sea Research II, this issue.

Griffin, D.A., Wilkin, J.L., Chubb, C.F., Pearce, A.F., Caputi., N., 2001. Ocean currents and the larval phase of Australian western rock lobster, *Panulirus cygnus*. Marine and Freshwater Research 52, 1187–1199.

Hormazabal, S., Núñez, S., Arcos, D., Espindola, F., Yuras, G., 2004. Mesoscale eddies and pelagic fishery off central Chile (33–40°S). Gayana 68 (2) supl. t.I. Proc., 291–296.

Le Traon, P.Y., Nadal, F., Ducet, N., 1998. An improved mapping method of multi-satellite altimeter data. Journal of Atmospheric and Oceanic Technology 25, 522–534.

Martin, A.P., Richards, K.J., 2001. Mechanisms for vertical nutrient transport within a North Atlantic mesoscale eddy. Deep-Sea Research II 48, 757–773.

McGillicuddy, D.J., Johnson, R., Siegel, D.A., Michaels, A.F., Bates, N.R., Knap, A.H., 1999. Mesoscale variations of biogeochemical properties in the Sargasso Sea. Journal of Geophysical Research: Oceans 104 (C6), 13,381–13,394.

Miller, L.A., Marie, R., Crawford, W.R., 2005. The large, westward-propagating Haida Eddies of the Pacific eastern boundary. Deep-Sea Research II 52, 845–851.

Mizobata, K., Saitoh, S.I., Shiomoto, A., Miyamura, T., Shiga, N., Imai, K., Toratani, M., Kajiwara, Y., Sasaoka, K., 2002. Bering Sea cyclonic and anticyclonic eddies observed during summer 2000 and 2001. Progress in Oceanography 55, 65–75.

Moore, T.S., Matear, R.J., Marra, J., Clementson, L., 2007. Phytoplankton variability off the Western Australian coast: mesoscale eddies and their role in cross-shelf exchange. Deep-Sea Research II, doi:10.1016/j.dsr2.2007.02.006.

Morrow, R., Fang, F., Fieux, M., Molcard, R., 2003. Anatomy of three warm-core Leeuwin Current eddies. Deep-Sea Research II 50, 2229–2243.

Morrow, R., Birol, F., Griffin, D., Sudre, J., 2004. Divergent pathways of cyclonic and anti-cyclonic ocean eddies. Geophysical Research Letters 31, L24311.

Nelson, D., McCarthy, J., Joyce, T., Ducklow, H., 1989. Enhanced near-surface nutrient availability and new production resulting from the frictional decay of a Gulf Stream warm-core ring. Deep-Sea Research 36, 705–714.

Oliveira, P.B., Peliz, A., Jesus, D., Rosa, T.L., Santos, A.M.P., 2003. Winter geostrophic currents and eddies in the western Iberia coastal transition zone. Deep-Sea Research I 51, 367–381.

Osgood, K.E., Bane, J.M., Dewar, W., 1987. Vertical velocities and dynamical balances in Gulf Stream meanders. Journal of Geophysical Research: Oceans 92, 13,029–13,040.

Paterson, H., Knott, B., Waite, A., 2007. Microzooplankton community structure and herbivory on phytoplankton, in an eddy pair in the Indian Ocean off Western Australia. Deep-Sea Research II, doi:10.1016/j.dsr2.2006.12.011.

Peliz, A., Dubert, J., Haidvogel, D.B., Le Cann, B., 2003. Generation and unstable evolution of a density–driven Eastern Poleward Current: the Iberian Poleward Current. Journal of Geophysical Research 108, 3268.

Peliz, A., Dubert, J., Santos, A.M.P., Oliveira, P.B., Le Cann, B., 2005. Winter upper ocean circulation in the Western Iberian Basin-fronts, eddies and poleward flows: an overview. Deep-Sea Research I 52, 621–646.

Phillips, B.F., 1981. The circulation of the southeastern Indian Ocean and the planktonic life of the western rock lobster. Oceanography and Marine Biology. Annual Review 19, 11–39.

Rennie, S.J., Pattiaratchi, C.P., McCauley, R.D., 2007. Eddy formation through the interaction between the Leeuwin Current, Leeuwin Undercurrent and topography. Deep-Sea Research II, doi:10.1016/j.dsr2.2007.02.005.

Thomas, H., Bozec, Y., Elkalay, K., de Baar, H.J.W., 2004. Enhanced open ocean storage of CO_2 from shelf sea pumping. Science 304, 1005–1008.

Thompson, R.O.R.Y., 1987. Continental-shelf-scale model of Leeuwin Current. Journal of Marine Research 45, 813–827.

Thompson, P., Pesant, S., Waite, A., 2007. Contrasting the vertical differences in the phytoplankton biology of a dipole pair of eddies in the south eastern Indian Ocean. Deep-Sea Research II, this issue.

Waite, A.M., Thompson, P.A., Pesant, S., Feng, M., et al., 2007. The Leeuwin Current and its eddies: an introductory overview. Deep-Sea Research II, this issue.